Atmos. Meas. Tech. Discuss., 8, 2767–2791, 2015
www.atmos-meas-tech-discuss.net/8/2767/2015/
doi:10.5194/amtd-8-2767-2015

Atmospheric Measurement Techniques Discussions
Open Access

Use of portable FTIR spectrometers for detecting greenhouse gas emissions of the megacity Berlin – Part 2: Observed time series of XCO_2 and XCH_4

F. Hase[1], M. Frey[1], T. Blumenstock[1], J. Groß[1], M. Kiel[1], R. Kohlhepp[2], G. Mengistu Tsidu[1,4], K. Schäfer[3], M. K. Sha[1], and J. Orphal[1]

[1]Karlsruhe Institute of Technology (KIT), Institute for Meteorology and Climate Research (IMK-ASF), Karlsruhe, Germany
[2]German Weather Service, Offenbach, Germany
[3]Karlsruhe Institute of Technology (KIT), Institute for Meteorology and Climate Research (IMK-IFU), Garmisch-Partenkirchen, Germany
[4]Department of Physics, Addis Ababa University, P.O. Box 1176, Addis Ababa, Ethiopia

Received: 19 February 2015 – Accepted: 24 February 2015 – Published: 13 March 2015

Correspondence to: F. Hase (frank.hase@kit.edu)

Published by Copernicus Publications on behalf of the European Geosciences Union.

Abstract

Five portable Bruker EM27/SUN FTIR spectrometers have been used for the accurate and precise observation of column averaged abundances of CO_2 and CH_4 around the megacity Berlin. In the first part of this work (Frey et al., 2015) we have presented the various measures that were undertaken to ensure that the observations are consistent between sites, accurate and precise. Here, we present the recorded time series of XCH_4 and XCO_2 and demonstrate that the CO_2 emissions of Berlin can be clearly identified in the observations. A simple dispersion model is applied which indicates a total strength of the Berlin source of about $0.8\,t\,CO_2\,s^{-1}$. In the Supplement of this work, we provide the measured dataset and auxiliary data. We hope that the model community will exploit this unique dataset for state-of-the art inversion studies of CO_2 and CH_4 sources in the Berlin area.

1 Introduction

The application of portable FTIR spectrometers for the observation of column-averaged CO_2 and CH_4 abundances holds great promises with respect to the quantification of sources and sinks of greenhouse gases on regional and smaller scales. Although in-situ measurements at the ground can be performed with unrivaled precision and accuracy, these measurements suffer from the fact that they detect local variations and so are heavily influenced by local contributions and by details of the vertical mixing. Use of in-situ measurements on different altitude levels (tall tower, aircraft) improves the representativeness considerably, but is a rather expensive approach. Current space based remote sensing observations are useful for the quantification of sources and sinks on continental scales, but still suffer from limited precision, limited density of observations, and biases related to details of atmospheric scattering properties. Ground-based observations using high-resolution laboratory spectrometers as performed by TCCON (Total Carbon Column Observing Network, Wunch et al., 2011) can provide

AMTD
8, 2767–2791, 2015

column averaged abundances with reference precision and accuracy, but the number of sites is limited and the stations are not mobile. Portable FTIR spectrometers therefore are a very promising complement to current techniques, because they can probe larger sample volumes than in-situ and smaller scales than current space-based sensors or globally distributed ground-based remote sensing networks. In this work, we demonstrate the approach of using solar absorption spectra recorded with small low-resolution FTIR spectrometers at several sites distributed around a source region for an estimation of the encircled source strength. The demonstration is based on a campaign we performed from 23 June 2014 to 11 July 2014 around Berlin using five spectrometers. The site locations are detailed in the first part of this work. Due to somewhat unfavourable weather conditions, we were able to perform simultaneous measurements at all sites only on 10 days during the demonstration campaign. However, it should be noted that such spectrometers can be installed for longer periods of operation in weather-resistant shelters and operated automatically – in order to from a permanent component of future monitoring systems.

Due to the long lifetimes of CO_2 and CH_4, each individual source contribution is a weak signal superimposed on the average column-averaged background abundance. Therefore, ensuring a common calibration of all involved spectrometers and demonstrating their instrumental stability is of utmost importance for the proposed method. In the first part of this work, we have described the rigorous calibration procedures we applied for the EM27/SUN spectrometers involved in this campaign and the excellent instrumental stability which our pre- and after campaign tests revealed.

2 Weather and prevailing winds and auxiliary measurements

In Table 1, we collect the main characteristics of each measurement day. We list the number of observations available at each site, and deduce a daily quality flag according to the overall data availability. Furthermore, the wind speeds and prevailing wind directions in the boundary layer are provided. The best measurement days with measure-

AMTD
8, 2767–2791, 2015

ments during throughout most of the day (solar elevation angle > 20°) were 27 June, 3 and 4 July. During these days, prevailing winds were from the West (and South). Wind speeds were moderate in the range of 5 to 8 kn. Note that although not very well covered, the set of observations includes a Sunday (6 July), which is an interesting aspect, as a different temporal pattern and overall strength of emissions is expected on a Sunday than during a working day.

A very important auxiliary information required for the proper estimation of a source strength is the development of the boundary layer height during each day of observations. IMK-IFU performed continuous ceilometer measurements of the boundary layer height during the whole campaign period. The measurements were performed in Berlin Neukölln (52.4895° N, 13.4309° E), 2.5 km to the southeast from the city center. The applied ceilometer CL51 from Vaisala GmbH, Hamburg, Germany, is an eye-safe commercial mini-lidar system. Ceilometers detect originally the cloud height, but special software provides routine retrievals of up to 5 lifted layers from vertical profiles (vertical gradient) of laser backscatter density data (Münkel, 2007). In the absence of low clouds and precipitation and during scattered clouds, this measurement method estimates boundary layer height fairly well. The CL51 detects convective layer depths exceeding 2000 m and nocturnal stable layers down to 50 m. The measurements results agree well with those which are determined from profiles of relative humidity and virtual potential temperature measured by radiosonde (location of strong height gradient of aerosol backscatter density and relative humidity as well as temperature inversion, see Emeis et al., 2012). But radiosondes which are launched routinely twice per day only do not provide sufficient information. Figure 1 shows the ceilometer results for 27 June: the developing boundary layer can be nicely seen, reaching an altitude of about 2200 m in the late afternoon. In the case of airborne particles it could be shown earlier that boundary layer information as detected continuously by ceilometers enables the determination of near-surface concentrations from column density data (Schäfer et al., 2008).

AMTD
8, 2767–2791, 2015

3 The XH_2O, XCO_2 and XCH_4 timeseries

Figure 2 shows the observed time series of H_2O dry air mole fractions. As expected, H_2O is varying considerably – by about a factor of three – over the campaign period. On the other hand, the agreement between the stations is surprisingly good. This demonstrates the uniform character of the selected area, especially the absence of localized dominating sources of atmospheric humidity, which would induce larger differences between the stations. Finally, as the main contribution to the H_2O total column originates from the boundary layer, this finding supports the assumption that the boundary layer across the whole probed area is well ventilated.

Figures 3 and 4 show the XCO_2 and XCH_4 values, respectively, as observed by all spectrometers. The dominating synoptic variations which are common to all sites occur on timescales of several days. These variations in the order of one per cent peak-to-peak are due to the changing tropopause altitude and advection of air masses with different trace gas concentrations. In addition, the time series reveal intraday variability in the order of 0.5 % or less, which is variable from day to day, but also very similar in each individual data record. We assume that these variations result from a superposition of real variability and artefacts of the retrieval. During most of the observation days, a decrease of XCO_2 is found, which is what would be expected as a result of photosynthetic activity during a sunny day (high insulation being an obvious selection bias of solar absorption observations). On the other hand, variations symmetric around noon are particularly striking during a couple of days, mainly in the case of CH_4. It is plausible to assume an airmass-dependent retrieval biases as a cause of these variations. We detailed in the first part of this work that we attempted to remove this artefact by applying an a-posteriori airmass-dependent correction. However, the observed bias will be comprised of two contributions: one contribution resulting from forward model errors (e.g. wrong line broadening parameters) – this tends to be a systematic feature and can be removed by the global correction we applied – and a second contribution due to the smoothing error of the retrieval. The column sensitivity of the scaling retrieval is a func-

AMTD
8, 2767–2791, 2015

tion of airmass, and so is the smoothing error. As described in the first part of this work, we used constant a-priori profile shapes in the retrievals, while the actual atmospheric profiles are variable. This gives rise to airmass-dependent artefacts which are variable from day to day. Finally, on top of this variable background, subtle differences between individual observations can be detected: these are typically of the order of 1 to 2‰ and it is tempting to assume that these are caused by local emission contributions. For illustration, Fig. 5 shows the XCH_4 and XCO_2 values observed during 27 June. Southerly winds prevailed during that day, and indeed the XCO_2 values observed in Heiligensee in the Northwest of Berlin are elevated. It is important to note that although the emission signals tend to be smaller than the observed intraday variability, enhancements as small as 0.5‰ are noticeable. This is possible because the detection of an enhancement can be based on the differences between the column-averaged mole fractions observed at different sites, if these are superimposed on a smoothly varying background traced by the observations of several upstream stations. This situation is realized if all sites observe similar advected larger scale variations. Note that at a given time during the day all sites perform measurements under nearly the same solar elevation angle and quite similar atmospheric conditions (atmospheric vertical profile shapes of trace gases). This reduces significantly retrieval biases between the stations, especially if the interpretation of the collected data is mainly based on differences between simultaneous observations of upstream and downstream stations. In detail, the observed XCH_4 enhancements differ from the XCO_2 enhancements, which is expected due to different sources. Moreover, the background of the XCH_4 seems less well defined and more variable. This meets the expectation: due to the likely presence of rural CH_4 sources around the conurbation area encircled with the stations and due to the stronger contrast between tropospheric and stratospheric mixing ratios of CH_4 higher variability is expected in the XCH_4 background field than in case of XCO_2. We feel that a sensible investigation of our XCH_4 observations would require a state-of-the-art high-resolution inversion model and we hope that the datasets made available in the Supplement of this work will be exploited in depth by the inverse model community.

AMTD
8, 2767–2791, 2015

Using a simple dispersion model, we will in the following focus on a more specific interpretation of the observed XCO_2 enhancements. In the next section, we describe the main characteristics of the dispersion model. In Sect. 5 we compare observations and model predictions.

4 Setup of a simple dispersion model

For a prediction of the differences in XCO_2 between different sites we have created a simple dispersion model. Within this modelling scheme, the Berlin source is mapped into a schematic area source spanned by 5 neighbouring rectangles, which contribute to the total source strength. The central rectangle reflects the city center, the four remaining rectangles reflect Charlottenburg and Spandau areas (western box), Reinickendorf and Pankau areas (northern box), Marzahn-Hellersdorf and Treptow-Köpenick areas (eastern/south-eastern box), and the Tempelhof-Schöneberg area (southern box). The geographical coordinates of each box and the percentage contribution to the total emission are listed in Table 2. The spatial extent and contribution of each box have been inspired by informations on population and traffic density provided by the bureau of statistics of Berlin-Brandenburg (http://www.stadtentwicklung.berlin.de).

The dispersion model uses analysed hourly horizontal wind fields from COSMO-DE, the convective-scale regional component of the numerical weather prediction system of the German Weather Service DWD (Baldauf et al., 2011). Due to the fact that we assume a distributed source region, we do not apply the COSMO wind field at full resolution, which is in the order of 2.8 km × 2.8 km, but use only 5 COSMO hourly wind profiles distributed over the observation area (in the center and the NW, NE, SW, SE corners of a square centered on Berlin with an edge length of about 20 km) and interpolate the winds between these reference wind profiles linearly along time and – assuming a Shepard inverse distance weighting with a power of two (Shepard, 1968) – in a horizontal plane.

AMTD
8, 2767–2791, 2015

The model is based on a strict Lagrangian perspective. It does not use a model grid, but instead transports emitted "molecules" according to the interpolated winds at their current locations. The generation rate of the "molecules" is proportional to the source strength, they are created at the ground level within one of the five emission regions described before. For each creation act, the region is selected by a random generator in accordance with the assumed contribution of the region, the starting position within the selected area is again chosen randomly. Within a selected region, the probability of emission is equal for each area element; we do not attempt to resolve sources on a scale smaller than the source region.

Concerning the vertical transport, a fast mixing on timescales of ~ 10 min across the whole boundary layer is assumed. This is realized in the model by introducing a fast erratic diffusion of each "molecule" along the vertical axis. The altitude limit of the model boundary layer is for each day chosen in accordance with ceilometer measurements. Fast fluctuations of the boundary layer thickness detected by the ceilometer are neglected, instead the individual overall development of the boundary layer height during each day is approximated using piecewise linear fits.

Finally, the detection of "molecules" is emulated by checking whether the "molecule" is inside a cylinder which wraps the line of sight of one of the observation sites. It should be noted that due to the daily apparent motion of the sun in the sky, the position of this cylinder is quite variable. If we assume a boundary layer thickness of 1500 m and start and end of observations at a solar elevation angle of 20°, then the top surface of the cylinder is shifted by 8 km westwards during the day, which is not negligible in comparison to the extent of the assumed source regions. Therefore, the line-of-sight used for the detection condition is updated in the model according to the astronomical conditions.

The simulation period starts at midnight. In each time step (1 s), a "molecule" is emitted and all existing "molecules" are transported. During daytime, as long as the solar elevation exceeds 20°, the number of detected molecules at each observation site is determined in intervals of 450 s. Typically, depending on wind speed, 20 000 to

AMTD
8, 2767–2791, 2015

40 000 “molecules” are traced at a given time (each emitted “molecule” is followed for up to a distance of 40 km from the Berlin center). The simulation run for each day is repeated 500 times and the results averaged to achieve a negligible statistical noise in the number of detection counts. Note that the model does not take into account emissions from the previous day. Typically, these aged emissions have left the region of interest before, but occasionally – if the wind speed is very low – it might happen that they reside for longer than 6 h in the observed area, or may return from outside the modelled area if the wind direction is changing. No attempt is made in the dispersion calculation to include the variable advected XCO_2 background, it only predicts the enhancements at each observation site due to the daily emissions of the local Berlin source.

5 Comparison of predicted and observed time series

In the following, we compare the XCO_2 measurements with results from the dispersion model for the three most favourable observation days. For all days, the Berlin CO_2 source strength was fixed to a plausible value of 800 kg CO_2 per second. The source strength was kept constant during the day, although one would certainly expect considerable intraday variability for different kinds of contributions, e.g. traffic peaking at around 8 a.m. and 5 p.m. (local time). Figures 6 to 8 show the observational and model results for 27 June, 3 and 4 July. For the first two days, the model enhancements are shown superimposed on a smooth polynomial background, which is reasonably well defined by the observations of the upstream stations. During the third day, 4 July, it is more difficult to estimate a smooth background level, as all stations, including the upstream stations, observe considerable variability. Therefore, for this day the predicted enhancements are shown superimposed on a constant 390 ppm background level.

The model prediction for 27 June is of acceptable quality. The enhancements before noon observed first in Charlottenburg and afterwards in Heiligensee are well captured. The peak at 0.35 day fraction observed in Heiligensee, is much sharper than the

AMTD
8, 2767–2791, 2015

model prediction and indicates a significant contribution of a localised source smaller than the assumed emission regions. Southerly winds prevailed during the day, so this source is probably located in model region 1. Indeed, the heat and power generating coal-fired plant Reuter West operated by Vattenfall AB with a peak thermal power of 774 MW (Ref: http://kraftwerke.vattenfall.de/powerplant/reuter-west) is located in this region and is the likely source of the observed emissions. Afterwards, the model predicts elevated values for Heiligensee until around noon, which is in good agreement with the observations, but it fails to predict the final enhancement observed in Heiligensee after noontime.

For 3 July the enhancements are smaller than those observed during 27 June. Still, the undulations predicted by the model are detectable in the Lindenberg time series reasonably well, although the first two peaks are underestimated and appear delayed by about half an hour. The final increase towards the third peak observed in the afternoon is nicely reproduced. The model predicts slightly higher values for Mahlsdorf than for Heiligensee and Lichtenrade, which is not supported by the observations, which instead indicate repeated peaks in the Heiligensee and Lichtenrade timeseries. Westerly winds were prevailing during that day, so for the station Lichtenrade emissions from Potsdam (not included in the model) are likely to contribute.

For 4 July the observed XCO_2 values are quite variable. An M-shaped disturbance extending over 5 h and observed at all stations before noon is most prominent feature. Southerly winds prevailed near ground and southwesterly winds in the free troposphere. While a similar shape is observed at all stations, there is a clear time lag of about 45 min between the occurrence of this disturbance between the upstream stations (Lichtenrade and Charlottenburg) and the downstream stations (Heiligensee and Lindenberg). This time lag agrees well with the delay expected for the advection of a disturbance in the background XCO_2 signal at a wind speed of about 13 kn across a distance of about 20 km between the sites. The variations between the stations are too strong to allow a judgement concerning the model prediction of a 0.5 ppm enhancement at Heiligensee and Charlottenburg.

AMTD
8, 2767–2791, 2015

Figure 9 shows the MACC prediction for XCO_2. A closer examination of the previous development of the XCO_2 field according to MACC indicates that the complex structure in the XCO_2 field around Berlin during that day are possibly the result of an entrainment of emissions from Western Germany and further sources nearer to Berlin. The example of 4 July demonstrates the limitations of a simple dispersion model which takes into account only the local source. A comprehensive exploitation of the information contained in the kind of measurements presented here would require state-of-the-art inverse modelling allowing for a resolved local source distribution nested into a much wider model area. Such a model configuration would include a reasonable description of variations due to advected XCO_2 contributions from outside the model area and associated larger-scale variations of column averaged abundances.

6 Dataset provided in the Supplement

In the Supplement of this work, we provide the complete set of quality filtered XCH_4 and XCO_2 observations collected during the campaign at all stations. The quality filter is based on the quality of the interferograms (average value and fluctuation of the DC value). For each site, we provide the apparent solar elevation angle of the measurement, the retrieved total column amount of H_2O and the XCH_4 and XCO_2 calibrated with respect to TCCON and corrected for the systematic spurious air mass dependence (column-averaged dry air mole fractions in ppm). In separate tables, we provide the a-priori profile shapes of CH_4 and CO_2 used for the scaling retrieval on the 49 model levels of the retrieval code (dry air mole fractions in ppm) and the averaging kernels matrices of dimension 49 × 49 for different solar zenith angles. These auxiliary data enable the user to estimate the smoothing error of the column-averaged abundances, especially the impact of the actual profile shape on XCH_4 and XCO_2. If the user wants to include the smoothing characteristics of the remote sensing observations in the comparison between observations and assimilation model we suggest including the kernel convolution directly in the model predictor.

AMTD
8, 2767–2791, 2015

7 Summary and outlook

We presented measurements of column averaged abundances of CH_4 and CO_2 recorded with five portable FTIR spectrometers during a measurement campaign of three weeks duration around Berlin in summer 2014. The results demonstrate that an array of well-calibrated, ground-based FTIR spectrometers allow the reliable detection of XCH_4 and XCO_2 enhancements due to local emissions in the range of one per mil. Application of a simple dispersion model indicates that the observations are compatible with an assumed source strength in the order of 800 kg CO_2 s^{-1} for the megacity Berlin. We believe that arrays formed with such spectrometers would be a very useful complement to existing in-situ and remote-sensing measurements for the quantification of sources and sinks of CH_4 and CO_2 on regional scales. We expect that a comprehensive inversion of local source contributions to the observed column averaged abundances will require state-of-the art nested model approaches which include a proper description of the variable advected background contributions. Such model studies could also be of great value for the design of monitoring networks (density and locations of stations) based on portable FTIR spectrometers.

The Supplement related to this article is available online at doi:10.5194/amtd-8-2767-2015-supplement.

Acknowledgements. We acknowledge support by the ACROSS research infrastructure of the Helmholtz Association.

We acknowledge the availability of XCO_2 maps from MACC-III. MACC-III is a Coordination & Support Action (2014–2015) funded by the European Union under the Horizon 2020 Programme, coordinated by the European Centre for Medium-Range Weather Forecasts and operated by a 36-member consortium. A. Butz kindly prepared the plot based on MACC-III data.

We are very thankful for the successful cooperation during the measurement campaign "Berlin Air quality and Ecosytem Research: Local and long-range Impact of anthropogenic and

AMTD
8, 2767–2791, 2015

Natural hydrocarbons" (BAERLIN2014), and especially the coordinators Boris Bonn and Erika von Schneidemesser, Institute for Advanced Sustainability Studies e.V., Potsdam, Germany.

We thank the German Weather Service (DWD) for providing the COSMO-DE analysis data which were used for the wind profiles in the dispersion model.

We acknowledge support by Deutsche Forschungsgemeinschaft and Open Access Publishing Fund of the Karlsruhe Institute of Technology.

The article processing charges for this open-access publication have been covered by a Research Centre of the Helmholtz Association.

References

Baldauf, M., Seifert, A., Förstner, J., Majewski, D., Raschendorfer, M., and Reinhardt, T.: Operational convective-scale numerical weather prediction with the COSMO model: description and sensitivities, Mon. Weather Rev., 139, 3887–3905, doi:10.1175/MWR-D-10-05013.1, 2011.

Emeis, S., Schäfer, K., Münkel, C., Friedl, R., and Suppan, P.: Evaluation of the interpretation of ceilometer data with RASS and radiosonde data, Bound-Lay. Meteorol., 143, 25–35, 2012.

Frey, M., Hase, F., Blumenstock, T., Groß, J., Kumar Sha, M., Kiel, M., Kohlhepp, R., Mengistu Tsidu, G., Schäfer, K., and Orphal, J.: Use of portable FTIR spectrometers for detecting greenhouse gas emissions of the megacity Berlin – Part 1: Instrumental line shape characterisation and calibration of a quintuple of spectrometers, Atmos. Meas. Tech. Discuss., 8, 2735–2766, doi:10.5194/amtd-8-2735-2015, 2015, 2015.

Münkel, C.: Mixing height determination with lidar ceilometers – results from Helsinki Testbed, Meteorol. Z., 16, 451–459, 2007.

Schäfer, K., Harbusch, A., Emeis, S., Koepke, P., and Wiegner, M.: Correlation of aerosol mass near the ground with aerosol optical depth during two seasons in Munich, Atmos. Environ., 42, 18, 4036–4046, 2008.

Shepard, D.: Proceedings of the 1968 ACM National Conference, 517–524, 23rd ACM National Conference, Las Vegas, NV, USA, 27–29 August 1968, doi:10.1145/800186.810616, 1968.

AMTD

8, 2767–2791, 2015

Wunch, D., Toon, G. C., Blavier, J.-F. L., Washenfelder, R. A., Notholt, J., Connor, B. J., Griffith, D. W. T., Sherlock, V., and Wennberg, P. O.: The Total Carbon Column Observing Network, Philos. T. R. Soc. A, 369, 2087–2112, doi:10.1098/rsta.2010.0240, 2011.

AMTD
8, 2767–2791, 2015

Table 1. Summary of all measurement days: number of observations at each site (Mahlsdorf, Charlottenburg, Heiligensee, Lindenberg, Lichtenrade), overall quality ranking of each day according to number of available observations and temporal coverage, ground wind speed and direction.

Date	# observations	quality	wind speed (kn)	wind direction
26 Jun 2014 (Th)	76/70/89/28/116	+	2 . . . 4	NNE
27 Jun 2014 (Fr)	273/233/237/186/182	+ + +	5	SSW . . . SSE
28 Jun 2014 (Sa)	0/37/0/0/0	o	7	SSW
1 Jul 2014 (Tu)	203/189/158/122/224	++	8	W
2 Jul 2014 (We)	106/128/92/76/129	+	9	W
3 Jul 2014 (Th)	316/358/320/354/357	+ + +	7	W
4 Jul 2014 (Fr)	545/509/545/652/511	+ + ++	7	SW . . . S
5 Jul 2014 (Sa)	0/93/0/0/0	o	5	SSW . . . SSE
6 Jul 2014 (Su)	329/265/346/252/385	++	5	W . . . SW
7 Jul 2014 (Mo)	10/74/28/98/130	+	8	SE . . . NW
8 Jul 2014 (Tu)	0/21/0/0/0	o	6	NE . . . E
9 Jul 2014 (We)	35/29/40/0/10	o	6 . . . 10	E . . . SSW
10 Jul 2014 (Th)	248/306/411/188/245	++	6. . . 12. . . 6	NE . . . E
11 Jul 2014 (Fr)	257/248/212/243/253	+	8	NE

AMTD
8, 2767–2791, 2015

Table 2. The five emission regions used in the dispersion model.

Box ID	area	NW corner	SE corner	% contribution
1	Charlottenburg and Spandau	52.5677 13.0753	52.5159 13.2550	25
2	Tempelhof-Schöneberg	52.4657 13.2304	52.3800 13.4275	15
3	Marzahn-Hellersdorf and Treptow-Köpenick	52.5531 13.4502	52.3927 13.6316	10
4	Reinickendorf and Pankau	52.6302 13.3046	52.5472 13.4721	10
5	city center	52.5472 13.2550	52.4657 13.4502	40

AMTD
8, 2767–2791, 2015

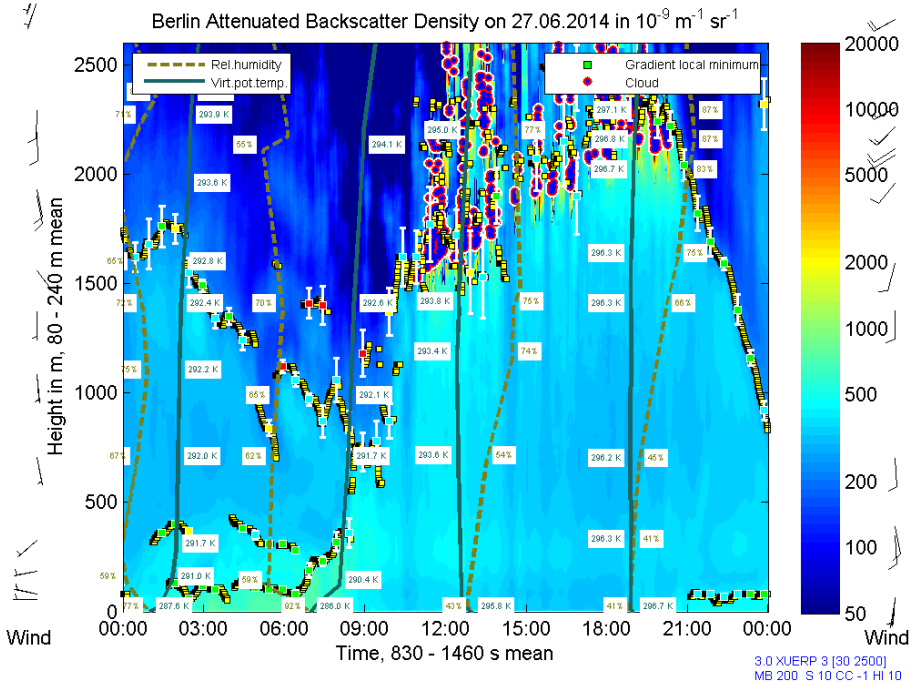

Figure 1. The development of the boundary layer thickness during 27 June according to ceilometer measurements performed by IMK-IFU in Berlin-Neukölln.

AMTD
8, 2767–2791, 2015

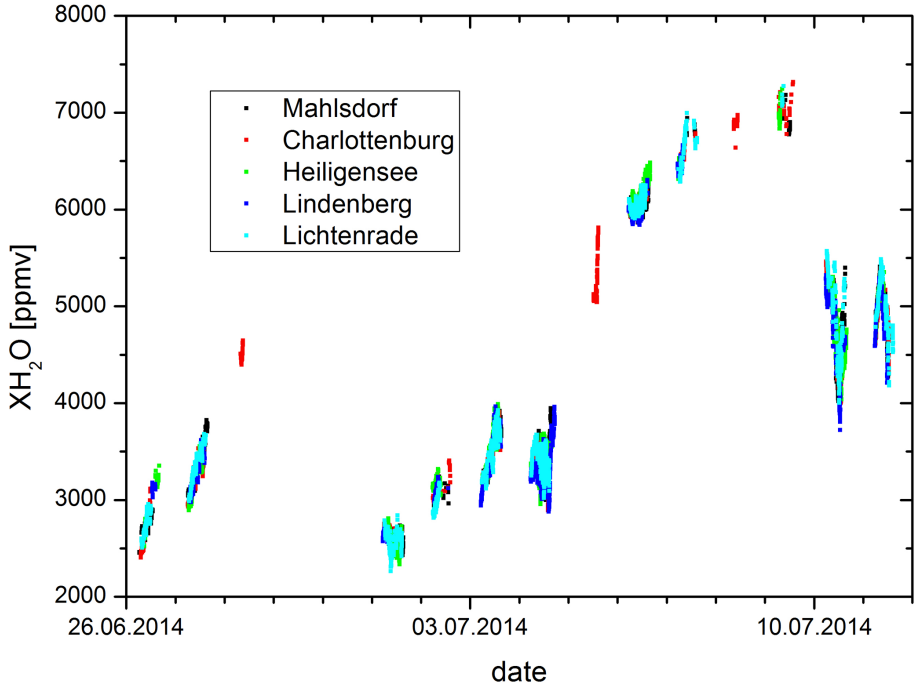

Figure 2. Evolution of $X\mathrm{H_2O}$ as measured at all sites during the campaign.

AMTD
8, 2767–2791, 2015

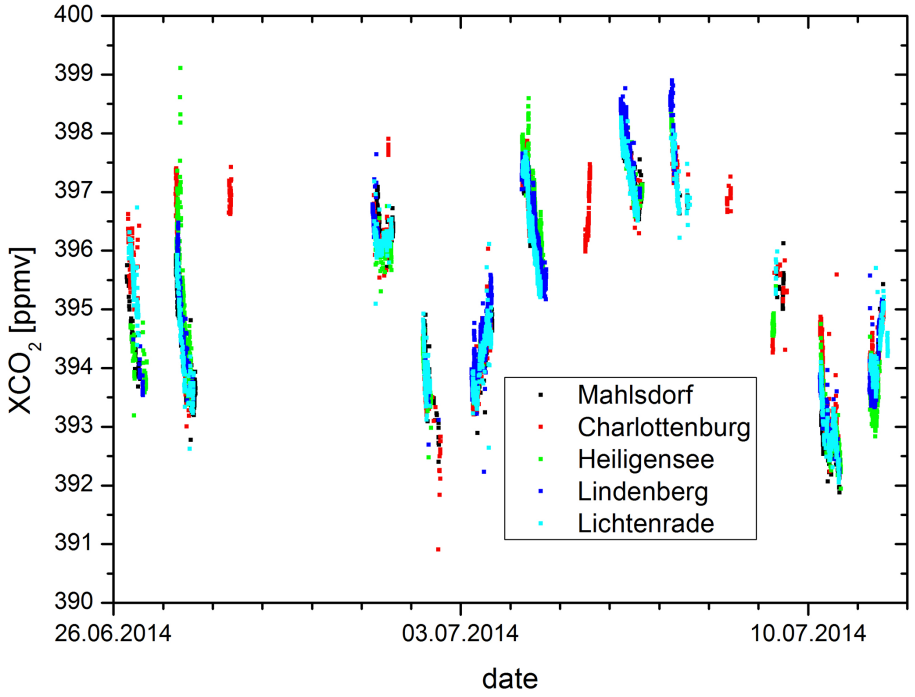

Figure 3. Evolution of XCO_2 as measured at all sites during the campaign.

AMTD
8, 2767–2791, 2015

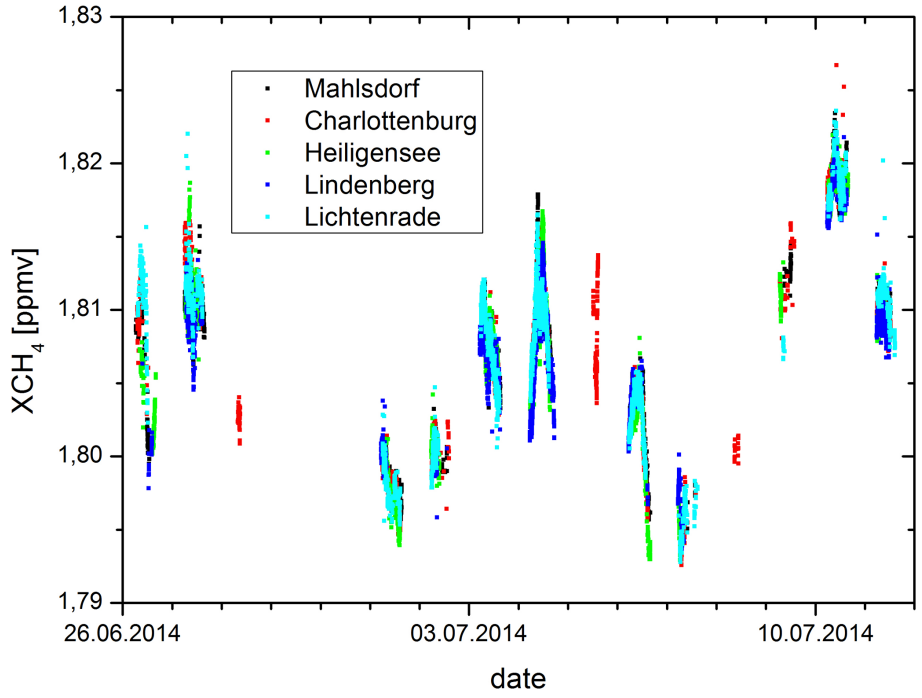

Figure 4. Evolution of XCH_4 as measured at all sites during the campaign.

AMTD
8, 2767–2791, 2015

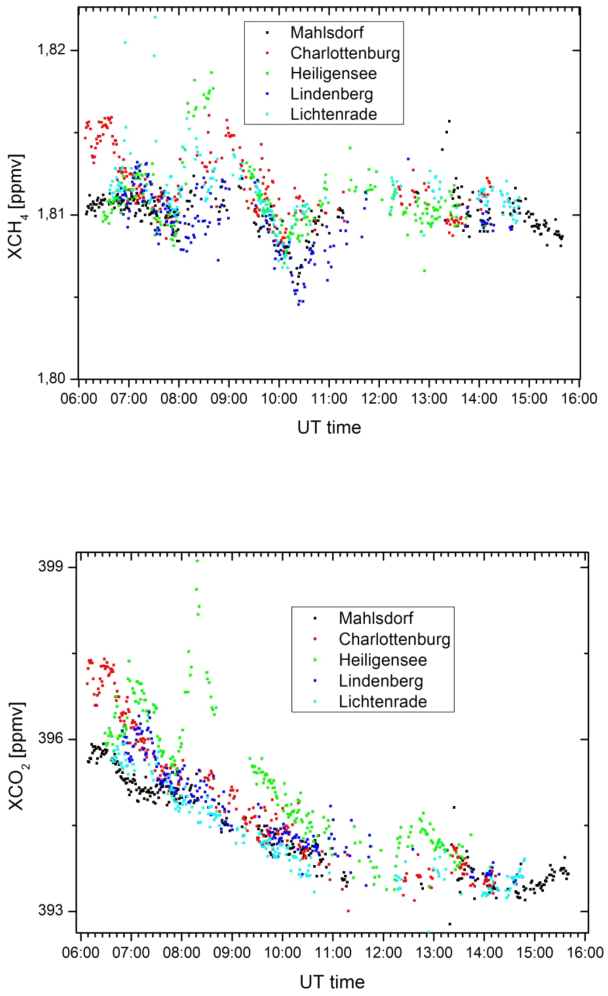

Figure 5. Observed variability of XCH_4 and XCO_2 during 27 June 2014.

AMTD
8, 2767–2791, 2015

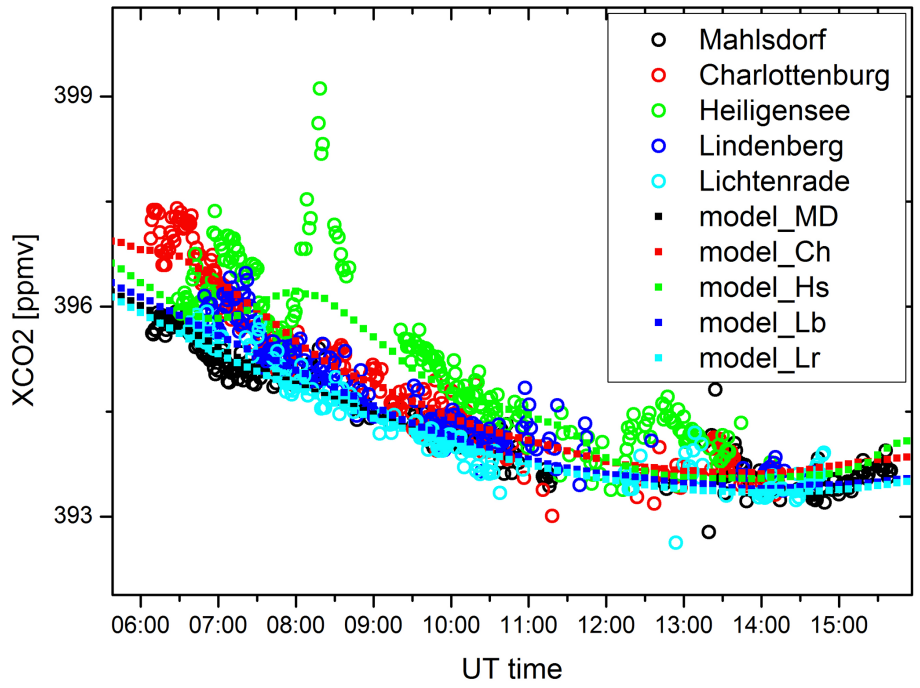

Figure 6. Observed and modelled XCO_2 for 27 June.

AMTD
8, 2767–2791, 2015

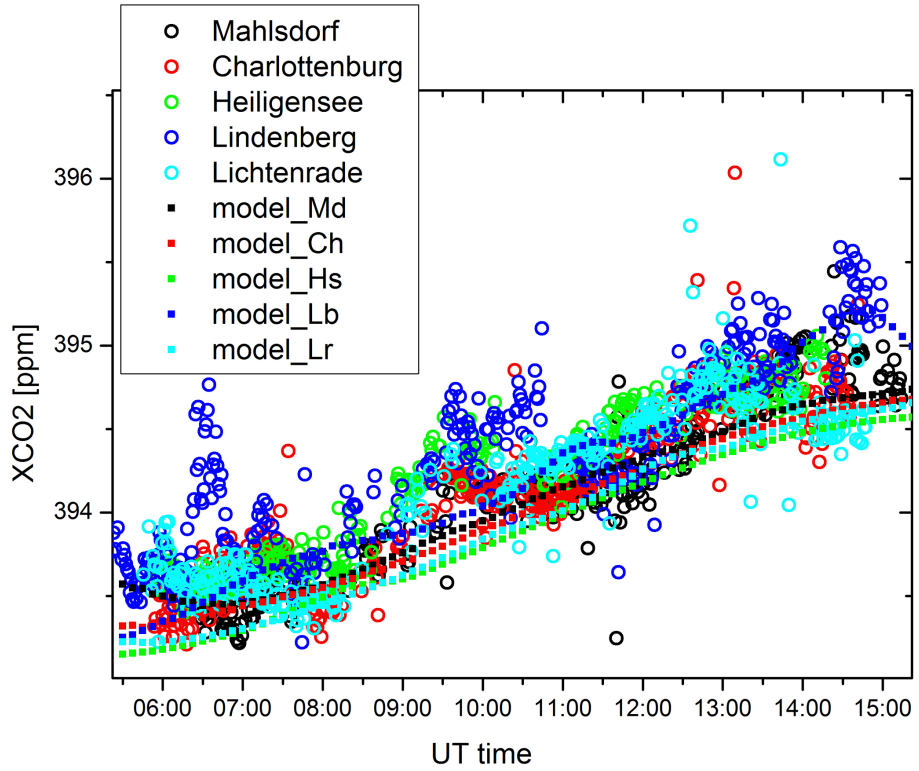

Figure 7. Observed and modelled XCO_2 for 3 July.

AMTD
8, 2767–2791, 2015

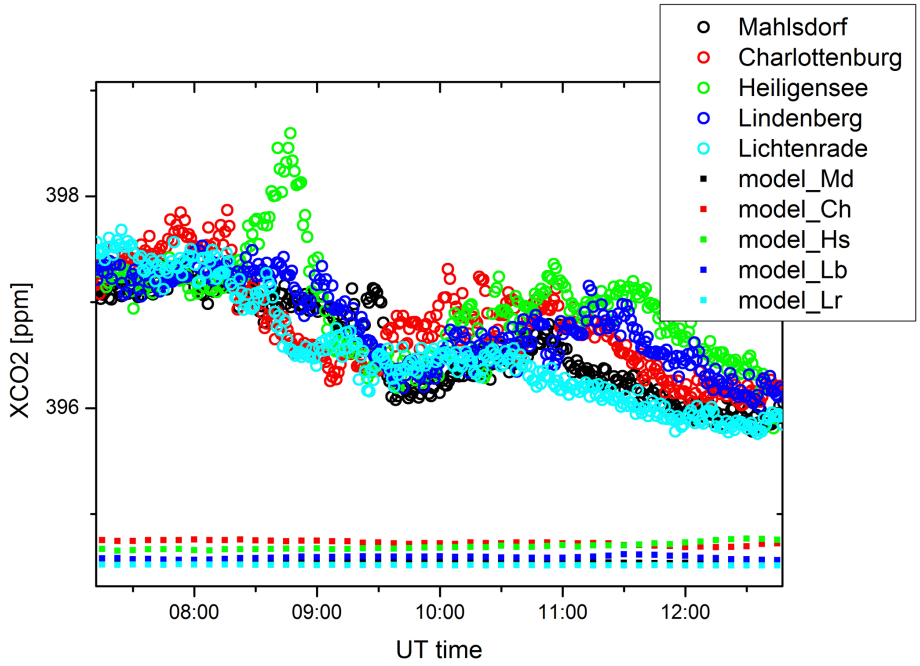

Figure 8. Observed and modelled XCO_2 for 4 July.

AMTD
8, 2767–2791, 2015

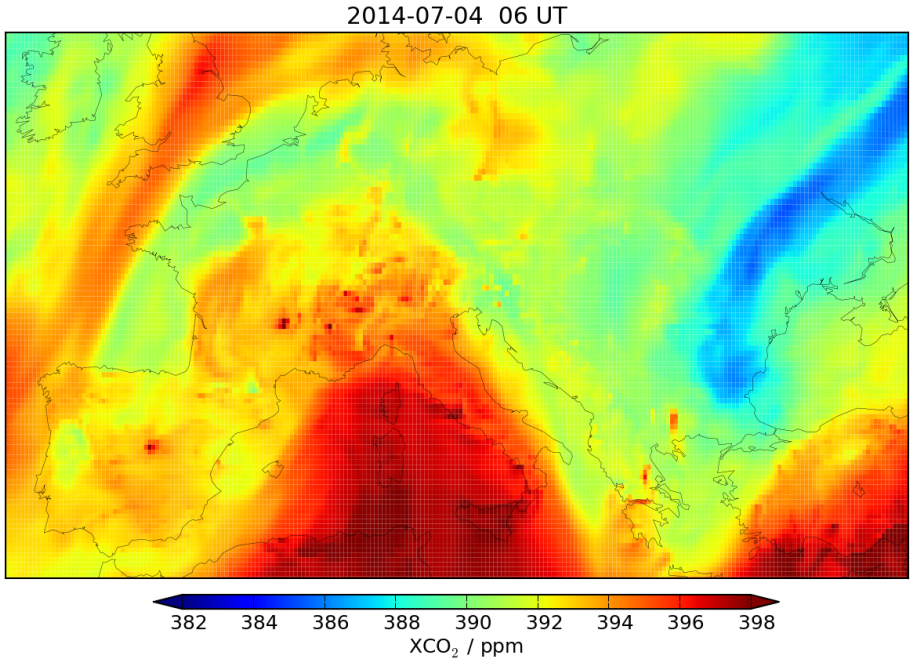

Figure 9. XCO_2 distribution according to the MACC model across central Europe for the morning of 4 July.

AMTD
8, 2767–2791, 2015